Three-dimensional time-dependent Hartree-Fock calculations of $^{16}O + {}^{16}O$ and $^{40}Ca + {}^{40}Ca$ fusion cross sections*

P. Bonche and B. Grammaticos†
Service de Physique Théorique, CEN-Saclay, B. P. No. 2, 91190 Gif-sur-Yvette, France

S. Koonin‡
The Niels Bohr Institute, University of Copenhagen, DK-2100 Copenhagen Ø, Denmark
and W. K. Kellogg Radiation Laboratory, California Institute of Technology, Pasadena, California 91125§

(Received 22 November 1977)

Three-dimensional time-dependent Hartree-Fock calculations for the $^{16}O + {}^{16}O$ and $^{40}Ca + {}^{40}Ca$ fusion excitation functions are presented. Results for the former system are in good agreement with experiment for $E_{lab} \leq 120$ MeV and indicate a dynamical lower angular momentum limit to fusion for $E_{lab} \geq 54$ MeV. Results for $^{40}Ca + {}^{40}Ca$ are compared with previous two-dimensional calculations. The low-energy fusion cross sections obtained for this system demonstrate the sensitivity of time-dependent Hartree-Fock calculations to the effective interaction used.

[NUCLEAR REACTIONS $^{16}O(^{16}O,x)$ and $^{40}Ca(^{40}Ca,x)$ calculated $\sigma_{fus}(E)$ in time-dependent Hartree-Fock approximation.]

I. INTRODUCTION

The time-dependent Hartree-Fock method (TDHF) is able to reproduce in a natural way the qualitative features of a variety of heavy-ion reaction phenomena.[1,2] The specific results of axially symmetric TDHF calculations[3-6] also give an encouraging microscopic and quantitative description of some experimental data. However, fully three-dimensional calculations which include nonaxial degrees of freedom seem to be necessary to fairly test certain aspects of the TDHF dynamics.[7-9] Of particular interest is whether or not there is sufficient one-body dissipation[10] associated with the time dependence of the mean field to account fully for experimental fusion cross sections. The crucial issues of the choice of effective interaction and the validity of axially symmetric calculations also remain largely unexplored.

In this paper, we present three-dimensional TDHF calculations in coordinate space for the systems $^{16}O + {}^{16}O$ and $^{40}Ca + {}^{40}Ca$ at a variety of bombarding energies and impact parameters. The $^{16}O + {}^{16}O$ calculations are complementary to the detailed study of this system at $E_{lab} = 105$ MeV by Flocard *et al.*,[9] while those for $^{40}Ca + {}^{40}Ca$ are directly comparable with previous two-dimensional work.[4] The range of initial conditions we cover allows us to make a fair and unambiguous comparison between the TDHF results and the experimental fusion excitation function for these systems. This is a stringent test of both the accuracy of the effective interactions we use and the overall validity of the TDHF description of heavy-ion reactions.

II. CALCULATIONAL METHODS

The theoretical foundations and basic numerical methods of our TDHF calculations have been adequately discussed elsewhere.[1,4,9] We impose a fourfold spin-isospin symmetry on the TDHF determinant. This is a valid assumption for the light systems we consider here.[11] The total energy of the determinant is expressed as a functional of the nucleon density ρ and kinetic energy density τ[4,5,9]:

$$E = \int d\vec{r}\left[\frac{\hbar^2}{2m}\tau(\vec{r}) + \frac{3}{8}t_0\rho^2(\vec{r}) + \frac{1}{16}t_3\rho^3(\vec{r})\right] + \frac{1}{2}V_0\int d\vec{r}\int d\vec{r}\,'\rho(\vec{r})\frac{\exp(-|\vec{r}-\vec{r}\,'|/a)}{|\vec{r}-\vec{r}\,'|/a}\rho(\vec{r}\,') + \frac{1}{8}e^2\int d\vec{r}\int d\vec{r}\,'\rho(\vec{r})\frac{1}{|\vec{r}-\vec{r}\,'|}\rho(\vec{r}\,'). \quad (1)$$

The first term in brackets is the kinetic energy, while the second and third terms are the expectation values of a Skyrme-type zero-range effective interaction with linear density dependence. The remaining terms in Eq. (1) arise from an internucleon Yukawa potential and the direct part of the Coulomb interaction. (The proton density is one-half of the nucleon density.)

Three different forces have been used in our calculations (Table I). They give identical nuclear matter parameters (saturation Fermi wave number = 1.29 fm^{-1}, saturation binding energy per nucleon = 15.85 MeV, incompressibility modulus = 368 MeV), but differ in their surface properties. Force I, which is almost identical to that used in Refs. 1, 4, 5, and 9, has a realistic surface energy

TABLE I. Properties of the effective interactions.

	Force I	Force II	Force III	Expt.
t_0 (MeV fm^3)	−497.73	−1099.0	−8.61	...
t_3 (MeV fm^6)	17 270.0	17 624.0	17 270	...
V_0 (MeV)	−363.04	0	−663.32	...
a (fm)	0.4598	...	0.4598	...
a_s (MeV)	18.7	8.4	24.0	24.7
d [c] (fm)	0.36	0.17	0.50	...
E/A [a] (^{16}O) (MeV)	7.15	9.78	5.54	7.98
E/A [a] (^{40}Ca) (MeV)	7.91	9.97	6.86	8.55
r_{ch} [b] (^{16}O) (fm)	2.73	2.58	2.85	2.73
r_{ch} [b] (^{40}Ca) (fm)	3.50	3.34	3.55	3.48
d [c] (^{40}Ca) (fm)	0.46	0.33	0.48	0.56

[a] Static HF binding energy per nucleon.
[b] Charge radius computed assuming an rms proton radius of 0.81 fm.
[c] 10–90% surface thickness.

coefficient (a_s) and surface thickness (d). These have been calculated for semi-infinite nuclear matter in the Thomas-Fermi approximation with Weizsäcker correction.[12] Force II is the zero-range force (no Yukawa term) used in Refs. 3, 7, and 8. It has an unphysically small surface energy coefficient and correspondingly sharp nuclear surfaces. Force III has been adjusted to have a large surface energy and a correspondingly diffuse nuclear surface. Also listed in Table I are the properties of the static HF solutions for the ^{16}O and ^{40}Ca ground states. These differences among the three forces result in often dramatic differences among the associated TDHF solutions.

Our numerical methods are similar to those of Ref. 9 but differ from them in detail. The TDHF determinant is constrained to be invariant with respect to both reflection through the reaction plane and inversion through the overall center of mass. The single-particle wave functions are described by their values on a uniform Cartesian mesh with a 1-fm mesh spacing in all three directions. The whole system is enclosed within a rectangular box with typical dimensions 30 fm × 20 fm × 16 fm for ^{16}O + ^{16}O and 30 fm × 30 fm × 20 fm for ^{40}Ca + ^{40}Ca, where the last dimension refers to the direction normal to the reaction plane. The numerical TDHF equations are derived by discretizing the energy functional (1) with the "five-point" difference approximation for the kinetic energy.[9] The single-particle wave functions are evolved in discrete time steps with the three-dimensional generalization of the alternating-direction method of Ref. 4. The double-stepping procedure of Refs. 1 and 4 is used to obtain the TDHF one-body Hamiltonian at the half time step. Time steps of $\Delta t = 4-5 \times 10^{-24}$ sec are used and the method is accurate through $\mathcal{O}(\Delta t^2)$. The one-body Coulomb and Yukawa potentials are obtained by solving iteratively the "three-point" Poisson and "five-point" Helmholtz problems with an alternating-direction technique.[13] The Coulomb boundary conditions are determined by an explicit evaluation of the Coulomb integral for selected points on the box faces, as in Ref. 4. Initial conditions are chosen to represent two identical ions in their static HF ground states with a relatively large separation ($\geq$10 fm for ^{16}O + ^{16}O, $\geq$ 14 fm for ^{40}Ca + ^{40}Ca) moving along the Coulomb trajectory they would have followed from far in the past. The static HF solution for a single nucleus is generated by either evolving the discrete TDHF equations with an imaginary time step[9] or by transcribing a large oscillator basis solution to the coordinate-space mesh. Our numerical methods conserve the total energy functional to within about 1 MeV and the normalization of the single-particle wave functions to within 1 part in 10^4 during a collision lasting 1.5×10^{-21} sec.

III. RESULTS

A. Comparison with axially-symmetric solutions

A typical TDHF fusion event is shown in Fig. 1, where we display contour plots of the nucleon density integrated over the direction normal to the scattering plane. The calculation has been done with force I for the ^{40}Ca + ^{40}Ca system at $E_{lab} = 278$ MeV with an initial orbital angular momentum $L = 40\hbar$. The general behavior of the density is similar to that found for ^{16}O + ^{16}O fusion events,[9] although the larger size of the system minimizes the effects of specific single-particle orbitals, which are dominant in lighter systems.[4,7-9]

The macroscopic dynamics in Fig. 1 is described conveniently by considering the coordinate frame defined by the instantaneous principal axes of the rigid-body inertia tensor. The reflection symme-

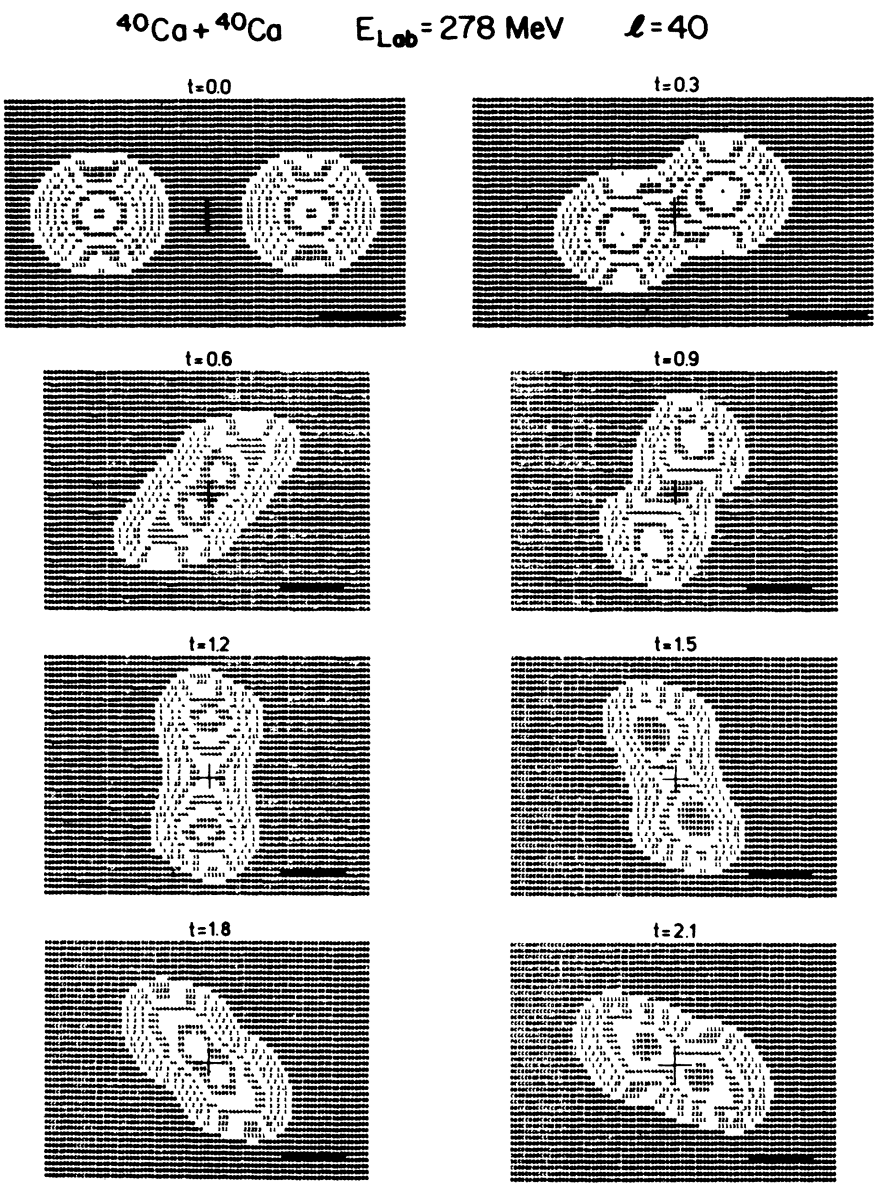

FIG. 1. Contour plots of the nucleon density integrated over the direction normal to the scattering plane for $^{40}Ca+^{40}Ca$ at $E_{lab}=278$ MeV, $L=40\hbar$. Force I has been used, and the time is given in units of 10^{-21} sec. The scale bar in the lower right corner of each time frame has a lenght of 5 fm and the cross indicates the time-independent position of the overall center of mass.

try of the determinant constrains one of these axes, z, to be normal to the reaction plane. The axis lying in the reaction plane associated with the larger eigenvalue is labeled y, and the remaining axis is labeled x. The fragment separation coordinate R may then be defined in terms of the moments of the density distribution as $R=2\langle|x|\rangle$.

Following the initial approach in Fig. 1, R passes through a minimum ($t=0.6\times10^{-21}$ sec) as the fragments "bounce" against an inner collective potential barrier of dynamical origin discussed Ref. 9, and begin to move apart ($t=0.9$–1.2×10^{-21} sec). However, the energy dissipated from radial collective motion into other degrees of freedom prevents scission and R passes through a maximum as the fragments again approach each other ($t=1.5$–1.8×10^{-21} sec). At later times (not shown) R continues to oscillate as the elongated compound system rotates. We define this behavior in our calculations as fusion and do not attempt to use TDHF to describe the subsequent decay of the compound nucleus. Since single-nucleon emission is forbidden by the spin-isospin and spatial symmetries we impose on the determinant and the validity of a

TDHF description decreases with increasing reaction time,[14] the later evolution of fusion events is treated more accurately by standard evaporation theory.

Our force I calculations for $^{40}Ca+^{40}Ca$ at $E_{lab}=278$ MeV are comparable directly to the axially symmetric results of Ref. 4. There is essential agreement at large impact parameters. The orbiting angular momentum was found to be $L=72\hbar$ in Ref. 4; it is $68-70\hbar$ in our three-dimensional calculations. The calculations also agree at small impact parameters, where the system does not fuse, but separates after the first minimum in R to give a highly inelastic event. However, at intermediate impact parameters, $25\hbar \lesssim L \lesssim 68\hbar$, our three-dimensional calculations do fuse where those in two dimenions do not.[4] An analysis of the three dimensional nuclear density shows that triaxial deformations are significant for these impact parameters. For example, in the $l=40$ collision of Fig. 1 the axial asymmetry, defined as $\langle z^2-y^2\rangle/\langle z^2+y^2\rangle$, reaches a value as large as 0.2. Together with the complete absence of fusion in the two-dimensional calculations, these results are a clear confirmation of the importance of nonaxial degrees of freedom in intermediate impact parameter events. They also provide a microscopic realization of the tangential dissipation introduced in macroscopic treatments.

B. $^{16}O+^{16}O$ fusion cross sections

Our global results for the $^{16}O+^{16}O$ system calculated with Force I are shown in Fig. 2. For bombarding energies in the range 20 MeV $\lesssim E_{lab} \lesssim$ 120 MeV we have determined the maximum fusion angular momentum $L_>(E_{lab})=l_>(E_{lab})\hbar$ with a precision of $1\hbar$. (The classical nature of TDHF permits all values of L, not only the even multiples of $\hbar$ permitted quantally.) This upper limit to fusion is well described by the expresion

$$l_>=\left[\frac{2\mu R_F^2}{\hbar^2}\left(\frac{E_{lab}}{2}-V_F\right)\right]^{1/2} \qquad (2)$$

in the range 20 MeV $\lesssim E_{lab} \lesssim$ 80 MeV. Here $\mu=8$ m is the reduced mass for the $^{16}O+^{16}O$ systems, $R_F=7.8$ fm is the fusion barrier radius, and $V_F=10.5$ MeV is the center-of-mass fusion barrier height. A comparison of V_F with the point-Coulomb interaction potential at R_F, 11.8 MeV, indicates that the nuclear ion-ion interaction is ~-1 MeV at this distance. These results are in agreement with those of Ref. 4 where the adiabatic $^{16}O+^{16}O$ potential was determined from axially symmetric TDHF calculations. For higher bombarding energies, $E_{lab}>80$ MeV, expression (2) overestimates $L_>(E_{lab})$ (by $4\hbar$ at $E_{lab}=120$ MeV), so that dynamical

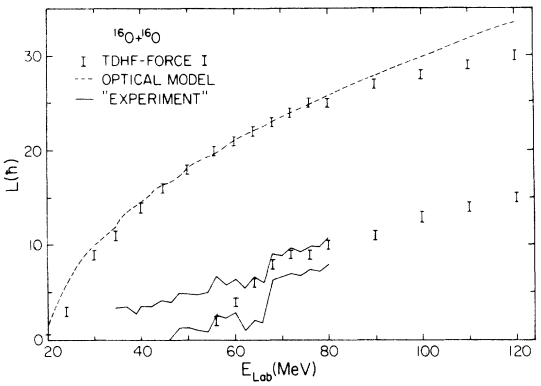

FIG. 2. Fusion limits for $^{16}O+^{16}O$. Upper and lower TDHF limits calculated with force I are indicated by the error bars. Also shown is the upper angular momentum limit extracted from the optical model total reaction cross section and the "experimental" lower angular momentum cutoff determined by the method described in the text. The uncertainty indicated in the experimental curve corresponds to the error bars of the data shown in Fig. 3.

effects appear to be important. Above $E_{lab}=E_0=54$ MeV low impact parameter events do not fuse but instead result in highly inelastic events, as described above for $^{40}Ca+^{40}Ca$. We have determined the lower fusion limit $L_<(E_{lab})=l_<(E_{lab})\hbar$ with a precision of $1\hbar$. This lower limit is well described by the expression

$$l_<=\left[\frac{2\mu R_B^2}{\hbar^2}\left(\frac{E_{lab}-E_0}{2}\right)\right]^{1/2}, \qquad (3)$$

where $R_B=4.1$ fm is the energy and angular momentum independent distance of closest approach (position of the inner barrier) for low impact-parameter events.[9] The form of Eq. (3) implies that all collisions with a radial velocity at R_B greater than some critical value will separate following their first elongation.

These results for the $^{16}O+^{16}O$ system are in disagreement with those of Ref. 8, where no fusion is found at $E_{lab}=128$ MeV (only a small extrapolation beyond the highest energy in Fig. 2). This discrepancy can be traced to the use of force II rather than force I and illustrates the importance of using an interaction with realistic surface properties. The smaller surface energy of force II enhances the low impact-parameter region of highly inelastic events by making scission following the first elongation easier. In addition, the lower surface energy and sharper nuclear surfaces resulting from this force raise the fusion barrier (see $^{40}Ca+^{40}Ca$ below). Both of these effects act to decrease the fusion cross section.

The TDHF results of Fig. 2 may be used to cal-

culate directly the fusion excitation function, without any phenomenological prescriptions to account for the lifetime of the compound nucleus as were introduced in Refs. 5 and 8. We compute the fusion cross section with the "sharp cutoff" formula, which is appropriate for the classical nature of the TDHF solutions:

$$\sigma_{\rm fus}(E_{\rm lab}) = \frac{2\pi}{k^2}\sum_l (2l+1) \qquad (4a)$$

$$\approx \frac{\pi\hbar^2}{\mu E_{\rm lab}}\left[(l_>+1)^2 - (l_<+1)^2\right]. \qquad (4b)$$

Here k is the wave number for the relative $^{16}O + ^{16}O$ motion and the sum is over all even partial waves which fuse. Equation (4b) approximates the quantal formula (4a) in a continuous manner in terms of $l_>$ and $l_<$. The TDHF excitation function is compared in Fig. 3 with the data of Ref. 15 and the 120-MeV point of Ref. 16 ($\sigma_{\rm expt}$). Our calculations reproduce the gross shape and overall magnitude of the experimental curve with no adjustable parameters. Also shown in Fig. 3 is the total reaction cross section $\sigma_{\rm opt}$ computed from an optical potential which fits the $^{16}O+^{16}O$ elastic scattering for $E_{\rm lab} \leq 70$ MeV.[17] Within the accuracy of our TDHF calculations, there is no evidence for or against the small-amplitude periodic structure found in both $\sigma_{\rm opt}$ and the data.

Our TDHF calculations resolve the discrepancy between $\sigma_{\rm opt}$ and $\sigma_{\rm expt}$ with highly inelastic events at small impact parameters, rather than in the more peripheral events. This can be seen in Fig. 2, where we have plotted the equivalent upper angular momentum limit determined from $\sigma_{\rm opt}$ by a relation similar to Eq. (4b) with $l_<=0$. This is in excellent agreement with the TDHF $l_>$ curve for $E_{\rm lab} \leq 80$ MeV, indicating both models have the same behavior in the higher partial waves. However, standard optical potentials have no provision

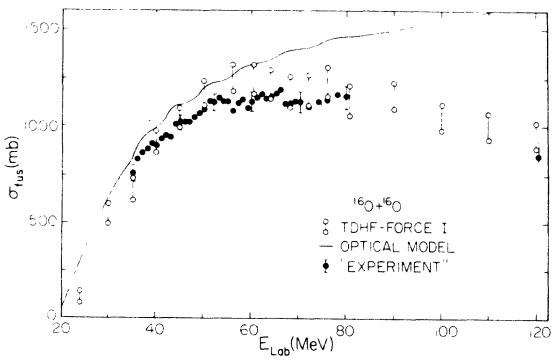

FIG. 3. Fusion excitation function for $^{16}O + ^{16}O$. The data are from Refs. 15 and 16, while the optical model is that of Ref. 17.

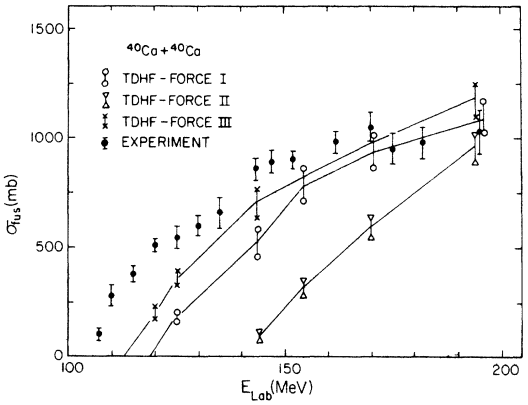

FIG. 4. Fusion excitation functions for $^{40}Ca+^{40}Ca$. The data are from Ref. 18. TDHF results with the various forces have been connected with straight lines to guide the eye.

for reproducing a lack of fusion in the low partial waves. The difference between $\sigma_{\rm opt}$ and $\sigma_{\rm expt}$ can then be used with Eq. (4b) to determine an "experimental" lower angular momentum fusion cutoff. This is also shown in Fig. 2, and is in good agreement with $l_<$ determined from the TDHF results.

C. $^{40}Ca + ^{40}Ca$ fusion cross sections

TDHF results for the $^{40}Ca+^{40}Ca$ fusion excitation function are compared with the data of Doubre *et al.*[18] in Fig. 4. For bombarding energies in the range 110 MeV $\leq E_{\rm lab} \leq$ 200 MeV, we have determined $L_>$ with a precision of $2-4\hbar$. We find no lower fusion cutoff in this energy range with any force. Since with force I $l_< \approx 25$ for $E_{\rm lab}=278$ MeV (see above), the highly inelastic events at low impact parameters must begin somewhere in the interval 200 MeV $< E_{\rm lab} <$ 278 MeV. All TDHF calculations are below the data throughout most of the range of comparison although they differ significantly among themselves. While the data can be described by Eqs. (2) and (4b) with $R_F = 10.2$ fm, $V_F = 51$ MeV, the TDHF calculations can be fitted with $R_F = 10.0$ fm and $V_F = 59$, 70, and 56 MeV, respectively, for forces I, II, and III. These differences are due to the different surface properties of the forces (Table I). Indeed, the 5% difference in rms radius and surface differences in the force I and force III ^{40}Ca solutions is sufficient to change V_F by 3 MeV.

The results presented above demonstrate the sensitivity of the calculated fusion cross section to the surface properties of the interaction. It therefore seems evident that TDHF can provide a quantitative description of experimental results, provided a force is used which describes correctly both nuclear matter and the simple surface properties of the reacting ions. A more sophisticated

energy functional than that used here, capable of simultaneously reproducing both the ^{16}O and ^{40}Ca ground states, should result in accurate fusion cross sections without any *ad hoc* modification of the force parameters.

IV. CONCLUSION

In summary, we have presented three-dimensional TDHF results for the $^{16}O+^{16}O$ and $^{40}Ca+^{40}Ca$ fusion excitation functions. For the former system, we obtain good agreement with experiment with no adjustable parameters. The TDHF approach therefore seems to contain sufficient dissipation to account for the data. Our calculations also show a dynamical lower angular momentum limit to fusion which is consistent with the data. This lower limit, should it exist in nature, is most likely due to the mass and spin-isospin symmetries of the experimental $^{16}O+^{16}O$ system and the approximate axial symmetry of nearly head-on collisions. All of these inhibit energy dissipation by reducing the number of relevant degrees of freedom. An alternative explanation of the difference between the experimental fusion cross section and the optical model total reaction cross section shown in Fig. 3 is inelastic scattering in the high partial waves due to a lack of high angular momentum compound nucleus states. It is therefore a challenging problem to distinguish experimentally these two very different situations.

For the $^{40}Ca+^{40}Ca$ system, we compared our three-dimensional solutions to calculations restricted to axial symmetry. Although agreement was found at both small and large impact parameters, nonaxial degrees of freedom are essential for a proper description of the intermediate partial waves. Our calculations of the fusion cross section near the Coulomb barrier are sensitive to the effective interactions used. Agreement with experiment can be improved by adjustment of the force parameters or presumably by using a more sophisticated form of the energy functional. The encouraging results presented here clearly warrant such improvements as well as the extension of our calculations to other light-ion systems.

We are grateful to the experimental groups at Orsay and the Neils Bohr Institute for encouraging these calculations and providing their data. M. Stillerman was helpful in the early stages of code development and the computational assistance furnished by C. Verneyre at Saclay and B. S. Nilsson at the Niels Bohr Institute has been essential to this work.

---

*Supported in part by the National Science Foundation (PHY76-83685) at Caltech.

†Also at CRN Strasbourg, 67 Kronenbourg, France.

‡Alfred P. Sloan Foundation Fellow.

§Permanent address.

[1]P. Bonche, S. Koonin, and J. W. Negele, Phys. Rev. C 13, 1226 (1976).

[2]P. Bonche, J. Phys. (Paris) 37, C5-213 (1976).

[3]S. Koonin, Phys. Lett. 61B, 227 (1976).

[4]S. E. Koonin, K. T. R. Davies, V. Maruhn-Rezwani, H. Feldmeier, S. J. Krieger, and J. W. Negele, Phys. Rev. C 15, 1359 (1977).

[5]V. Maruhn-Rezwani, K. T. R. Davies, and S. E. Koonin, Phys. Lett. 67B, 134, (1977).

[6]H. Flocard, S. E. Koonin, P. Møller, J. R. Nix, J. W. Negele, and A. Sierk, Phys. Rev. C (to be published).

[7]R. Y. Cusson, R. K. Smith, and J. Maruhn, Phys. Rev. Lett. 36, 1166 (1976).

[8]R. Y. Cusson, J. A. Maruhn, and H. W. Meldner, Oak Ridge National Laboratory Report, April, 1977 (unpublished).

[9]H. Flocard, S. E. Koonin, and M. Weiss, Phys. Rev. C 17, 1682 (1978), preceding paper.

[10]J. Blocki, Y. Boneh, J. R. Nix, J. Randrup, M. Robel, A. J. Sierk, and W. J. Swiatecki, Lawrence Berkeley Laboratory Report No. LBL-6536, 1977 (unpublished); S. E. Koonin, R. Hatch, and J. Randrup, Nucl. Phys. A283, 87 (1977); S. E. Koonin and J. Randrup, Nucl. Phys. A289, 475 (1977).

[11]J. Maruhn and R. Y. Cusson, Nucl. Phys. A270, 437 (1976).

[12]C. F. v. Weizsäcker, Z. Phys. 96, 431 (1935).

[13]J. Douglas, Jr., Numer. Math. 4, 41 (1962).

[14]P. C. Lichtner and J. J. Griffin, Phys. Rev. Lett. 37, 1521 (1976).

[15]B. Fernandez, C. Gaarde, J. Larsen, S. Sørensen, and F. Videbaek (unpublished).

[16]M. Conjeaud, S. Harar, F. Saint-Laurent, J. M. Loiseaux, J. Menet, and J. B. Viano, Proceedings of the International Conference on Nuclear Structure, Tokyo, 1977 (unpublished), p. 663; S. Harar (private communication).

[17]R. H. Siemssen, in Proceedings of the Argonne Symposium on Heavy-Ion Scattering [Argonne National Laboratory, 1971 (unpublished)], ANL Report No. 7837, p. 145.

[18]H. Doubre, A. Gamp, J. C. Jacmart, N. Poffé, J. C. Roynette, and J. Wilczyński, Orsay Report No. IPNO-PhN-77-26, October, 1977 (unpublished); H. Doubre (private communication).

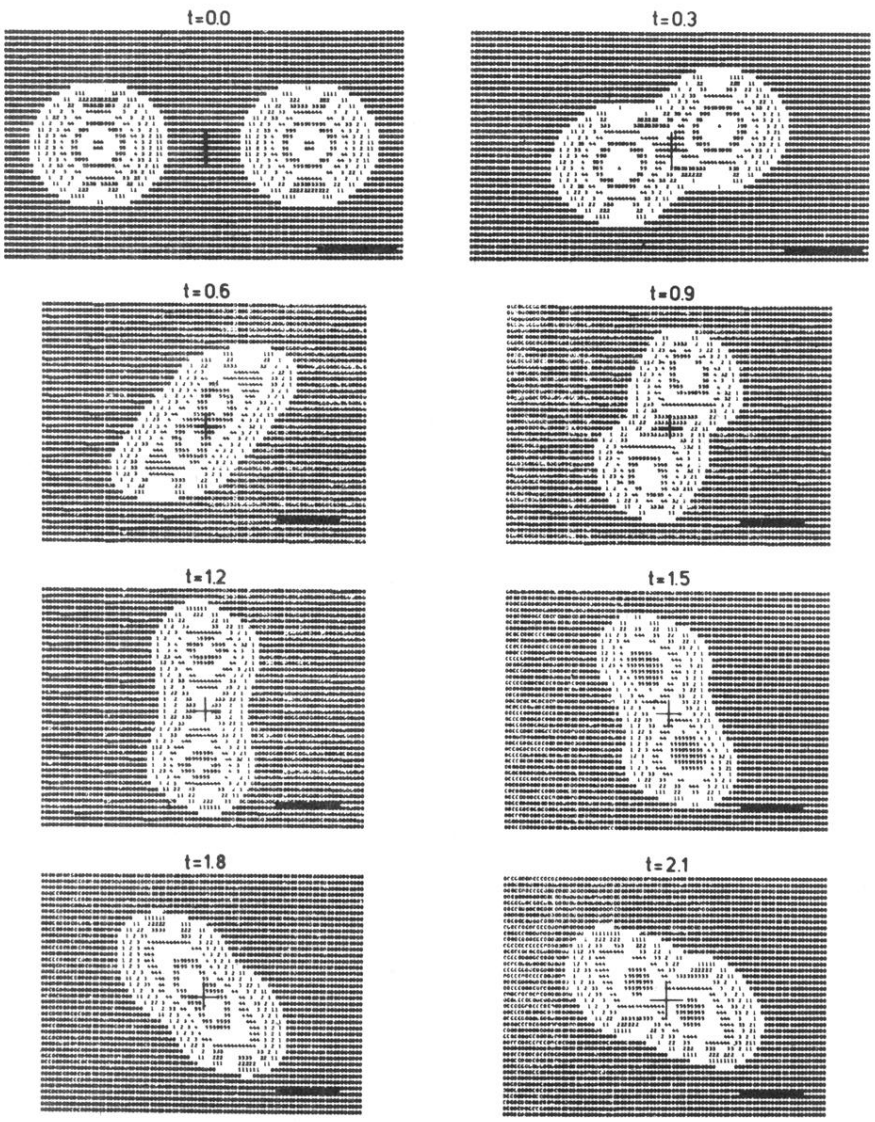

FIG. 1. Contour plots of the nucleon density integrated over the direction normal to the scattering plane for $^{40}Ca + ^{40}Ca$ at $E_{lab} = 278$ MeV, $L = 40\hbar$. Force I has been used, and the time is given in units of 10^{-21} sec. The scale bar in the lower right corner of each time frame has a lenght of 5 fm and the cross indicates the time-independent position of the overall center of mass.